Published in IET Computer Vision
Received on 15th January 2013
Revised on 24th June 2013
Accepted on 14th July 2013
doi: 10.1049/iet-cvi.2013.0011

ISSN 1751-9632

Single image haze removal using content-adaptive dark channel and post enhancement

Bo Li, Shuhang Wang, Jin Zheng, Liping Zheng

School of Computer Science and Engineering, Beihang University, XueYuan Road No. 37, HaiDian District, Beijing 100191, People's Republic of China
E-mail: xiaohangpp@hotmail.com

Abstract: As a challenging problem, image haze removal plays an important role in computer vision applications. The dark channel prior has been widely studied for haze removal since it is simple and effective; however, it still suffers from over-saturation, artefacts and dark-look. To resolve these problems, this study proposes a method of single image haze removal using content-adaptive dark channel and post enhancement. The main contributions of this work are as follows: first, an associative filter, which can transfer the structures of a reference image and the grey levels of a coarse image to the filtering output, is employed to compute the dark channel efficiently and effectively. Secondly, the dark channel confidence is utilised to restrict the dark channel based on the content of the image. Finally, a post enhancement method is devised to map the luminance of the restored haze-free image with the preservation of local contrast. Experimental results demonstrate that the proposed method significantly improves the visibility of the hazy image.

1 Introduction

Owing to atmospheric absorption and scattering, the irradiance received by the camera from the scene point is attenuated along the line of sight and the incoming light is blended with the airlight. This phenomenon, called haze or fog, can significantly degrade the visibility of the scene. Most computer vision applications, such as image segmentation and object tracking, usually suffer from the poor visibility of the hazy images [1–3]. Therefore haze removal is highly desired in many practical applications. In general, the haze is highly related to the scene depth. As it is hard to estimate the scene depth from a single image, early haze removal methods usually require multiple input images or additional information [4–8]. However, it is impossible to fulfill the requirement in many situations, so that single image methods are proposed based on strong priors or assumptions [9–13].

Recently, single image haze removal has progressed significantly. Some methods improve the image visibility by contrast enhancement [11, 14–17]. These methods usually do not consider the scene depth, and therefore they cannot remove the haze naturally with the variation of the scene depth. For instance, Tan's method [11] improves the visibility considerably by maximising the local contrast, but the results often look unnatural because of over-enhancement. Some other methods perform haze removal by image restoration. Fattal's method assumes that the transmission and the surface shading are locally uncorrelated, which is physically sound but cannot handle heavy haze well [10]. He *et al.* [9] propose the dark channel prior, that is, most local patches in the outdoor haze-free image contain some pixels whose intensity is very low in at least one colour channel, and they remove the haze by simply reducing the dark channel to zero.

The dark channel prior is simple but effective for single image haze removal. Based on the work of He *et al.* [9], many methods have been proposed using the dark channel prior [9, 13, 14, 18]. However, it is quite possible that some areas of the image do not fulfill the dark channel prior, and it is not an easy task to calculate the dark channel. As a result, these methods may suffer from one or more of the following problems. First, some methods usually result in colour over-saturation, because they cannot satisfy the limit requirement that the obtained dark channel should be no brighter than the minimum colour channel. Secondly, these methods usually introduce artefacts into the smooth areas where the dark channel prior is unreliable. Finally, the restored haze-free image usually looks dark after haze removal, in that the irradiance from the scene point is attenuated during its propagation.

To resolve the three aforementioned problems, we propose the method of single image haze removal using content-adaptive dark channel and post enhancement. The main contributions of this work are as follows: first, in order to obtain the dark channel efficiently and effectively, we propose the associative filter, which can transfer the structures and the grey levels, respectively, of two input images to the filtering output. Secondly, we propose the dark channel confidence to restrict the dark channel according to the content of the image. Finally, inspired by the characteristics of the restored haze-free images, we devise the post enhancement method to map the luminance with the local contrast preserved. Compared with the

state-of-the-art, experimental results demonstrate that the proposed method yields satisfactory results on varied hazy images.

The remainder of this paper is organised as follows. The next section presents the observation on the problems of the existing methods. Section 3 gives the definition of the associative filter, the concept of the dark channel confidence, and the process of haze removal using the content-adaptive dark channel. Section 4 discusses the characteristics of the restored haze-free images and describes the post enhancement method, followed by Section 5 where comparison experiments are conducted against some state-of-the-art methods. Finally, the conclusion is drawn in Section 6.

2 Observation

The atmospheric scattering model, which is often simplified as (1), is widely used for haze removal [4, 19, 20]. The methods using the dark channel prior calculate the transmission $t(x, y)$ and the restored haze-free image, respectively, by (2) and (3). The restored haze-free images are prone to suffer from over-saturation, artefacts and dark-look, as shown in Fig. 1. In this section, we present the observation on the three problems

$$I^{c}(x, y) = J^{c}(x, y)t^{c}(x, y) + A^{c}\left(1 - t^{c}(x, y)\right) \tag{1}$$

$$\begin{aligned} t^{c}(x, y) &= 1 - \min_{c\in\{R,G,B\}}\left(\min_{(i,j)\in\Omega(x,y)}\left(\frac{I^{c}(i, j)}{A^{c}}\right)\right) \\ &= 1 - \frac{I_{dark}(x, y)}{A^{c}} \end{aligned} \tag{2}$$

$$J^{c}(x, y) = A^{c} + \frac{I^{c}(x, y) - A^{c}}{t^{c}(x, y)} \tag{3}$$

where $I(x, y)$ indicates the image captured by the camera, $J(x, y)$ indicates the haze-free image, A is the atmospheric airlight, $t(x, y)$ represents the portion of the light that is not scattered, $c \in \{R, G, B\}$ represents the colour channel index, Ω indicates the local patch centred at (x, y), and $I_{dark}(x, y)$ is the dark channel.

Fig. 1 *Results of the methods using the dark channel prior*

a Input haze images

b Restored results obtained, respectively, by Chu *et al.* [19], Pei *et al.* [13] and He *et al.* [10] from the top down. Top of *b*: the image is seriously over saturated. Middle of *b*: the artefacts are introduced into the smooth areas. Bottom of *b*: the details are hard to observe because of dark-look

IET Comput. Vis., 2014, Vol. 8, Iss. 2, pp. 131–140
doi: 10.1049/iet-cvi.2013.0011

First, we find that over-saturation is mainly because of the estimated dark channel $I_{\text{dark}}(x, y)$ being brighter than the minimum colour channel $I_{\min}(x, y) = \min_{c\in\{R,G,B\}} I^c(x, y)$. For example, some methods compute the dark channel using the bilateral filter or the median filter [13, 21], resulting in about half of the pixels' dark channel being brighter than the minimum colour channel. Theoretically, the dark channel should be no brighter than the minimum colour channel. In order to obtain the dark channel meeting this requirement, we propose the associative filter.

Secondly, the methods using the dark channel prior are prone to bring artefacts into these two kinds of areas, that is, the smooth areas, such as the grey roads and the white walls, and the areas where it is impossible to restore the details because of serious atmospheric scattering, especially for the images compressed by JPEG. Based on the observation that the applicability of the dark channel depends on the content of the image, we introduce the dark channel confidence, which is used to restrict the dark channel by considering the content of the image.

Finally, the lightness from the scene point is usually inadequate because of atmospheric scattering, so that the intensity of the restored haze-free image is very low. It is necessary to perform post enhancement on the restored haze-free image. However, the traditional methods, such as histogram equalisation, cannot make good use of the characteristics of the restored haze-free image. Although the restored haze-free image looks dark, its local contrast is indeed improved. Therefore, we propose the post enhancement, which can extend the dynamic range of the dark areas while preserving the local contrast.

3 Haze removal

In this section, we present the technique details of haze removal, consisting of four steps. First, we obtain the dark channel using the associative filter. Secondly, we explicitly give the definition of the dark channel confidence. Then, we calculate the airlight based on the work of [9], and we finally remove the haze using the content-adaptive dark channel.

3.1 Definition of the associative filter

As given in [22], the joint bilateral filter uses a spatial filter kernel and a range filter kernel, which are, respectively, fixed by two different images. The proposed associative filter, however, only uses a range filter kernel fixed by a coarse image and a reference image. The associative filter is able to transfer the structures of the reference image and the grey levels of the coarse images to the filtering output, as Fig. 2 illustrates.

In general, the key idea of the associative filter is: the filtered result is the weighted average of the coarse image, and the weight is negatively related to the difference of the pixels between the coarse image and the reference image. The definition of the associative filter $\text{AF}(x, y)$ is given by

$$\text{AF}(x, y) = \frac{1}{W(x, y)} \sum_{(i,j)\in\Omega} \left(\exp\left(\frac{-(\text{AF}^{\text{cs}}(i, j) - \text{AF}^{\text{rf}}(x, y))^2}{2\sigma^2} \right) \text{AF}^{\text{cs}}(i, j) \right) \tag{4}$$

where $\text{AF}(x, y)^{\text{cs}}$ is the coarse image, $\text{AF}(x, y)^{\text{rf}}$ is the reference image, the size of the local patch Ω and the value of σ are set empirically, the normalisation factor $W(x, y)$

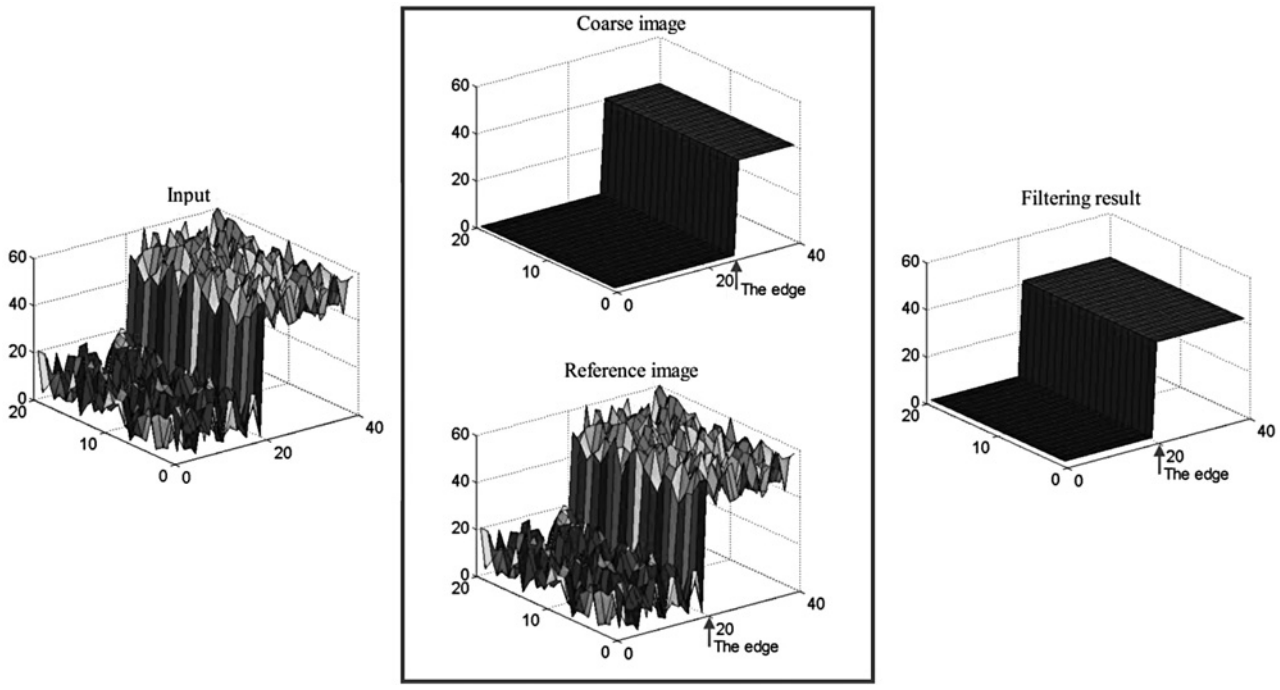

Fig. 2 *Illustration of the associative filter*

Edges of the coarse image, the reference image and the filtering result are, respectively, 25, 20 and 20
Brightest grey levels of the three images are, respectively, 40, 60 and 40. After filtering, the edges of the reference image and the grey level of the coarse image are transferred to the filtering result

ensures pixel weights sum to 1.0

$$W(x,y)=\sum_{(i,j)\in\Omega}\exp\left(\frac{-\left(\mathrm{AF}^{cs}(i,j)-\mathrm{AF}^{rf}(x,y)\right)^2}{2\sigma^2}\right) \quad (5)$$

As the weights of the associative filter only depend on the difference in value of the pixels, we can create a 255×255 table to storage the weights between different grey levels and then fix the weights by looking up the table. Moreover, the table is diagonally symmetric, so we only need to compute half of the values. As a result, the complexity of the associative filter is much lower than that of the joint bilateral filter, which takes into account the spatial distance between the pixels, especially for an image of large dimensions.

3.2 Dark channel computation

By substituting the coarse dark channel $I^{cs}_{dark}(x,y)$ and the minimum colour channel $I_{min}(x,y)$, respectively, for the coarse image and the reference image into (4), we can obtain the refined dark channel $I_{dark}(x,y)$

$$I_{dark}(x,y)=\frac{1}{W_{dark}(x,y)}\times\sum_{(i,j)\in\Omega}\left(\exp\left(\frac{-\left(I^{cs}_{dark}(i,j)-I_{min}(x,y)\right)^2}{2\sigma^2}\right)I^{cs}_{dark}(i,j)\right) \quad (6)$$

$$I^{cs}_{dark}(x,y)=\min_{(i,j)\in\Omega'}\left(\min_{c\in\{R,G,B\}}I^{c}(i,j)\right)=\min_{(i,j)\in\Omega'}\left(I_{min}(i,j)\right) \quad (7)$$

where σ is empirically set as 7, the size of the local patch Ω' is set as 15×15 according to [9].

It is obvious that

$$I^{cs}_{dark}(x,y)\le I_{min}(i,j),\quad (i,j)\in\Omega'(x,y) \quad (8)$$

Accordingly, it is easy to verify that

$$I_{min}(x,y)\ge I^{cs}_{dark}(i,j),\quad (i,j)\in\Omega'(x,y) \quad (9)$$

Then, we can obtain

$$\begin{aligned}I_{min}(x,y)&=\frac{1}{W_{dark}(x,y)}\times\sum_{(i,j)\in\Omega'}\left(\exp\left(\frac{-\left(I^{cs}_{dark}(i,j)-I_{min}(x,y)\right)^2}{2\sigma^2}\right)I_{min}(x,y)\right)\\&\ge\frac{1}{W_{dark}(x,y)}\times\sum_{(i,j)\in\Omega'}\left(\exp\left(\frac{-\left(I^{cs}_{dark}(i,j)-I_{min}(x,y)\right)^2}{2\sigma^2}\right)I^{cs}_{dark}(i,j)\right)\end{aligned} \quad (10)$$

As $I_{dark}(x,y)$ is the weighted average of $I^{cs}_{dark}(i,j)$ in the local area $\Omega(x,y)$, we can obtain the result that $I_{dark}(x,y)\le I_{min}(x,y)$ when the size of Ω is the same as that of Ω'.

In order to remove the unnecessary textures, we empirically set the size of Ω in (6) as 40×40. Even so, the dark channel is no brighter than the minimum colour channel for more than 95% pixels tested on 110 images. Since the block effect of the coarse image occurs in the areas where the coarse image and the reference image have obvious differences, the associative filter is effective at eliminating the block effect of the coarse image.

Fig. 3 presents an example using the associative filter. We can see that the associative filter not only preserves the structures of the minimum image well, but also removes the block effect and unnecessary textures. In addition, the grey level of every pixel in Fig. 3*c* is no brighter than that in Fig. 3*a*.

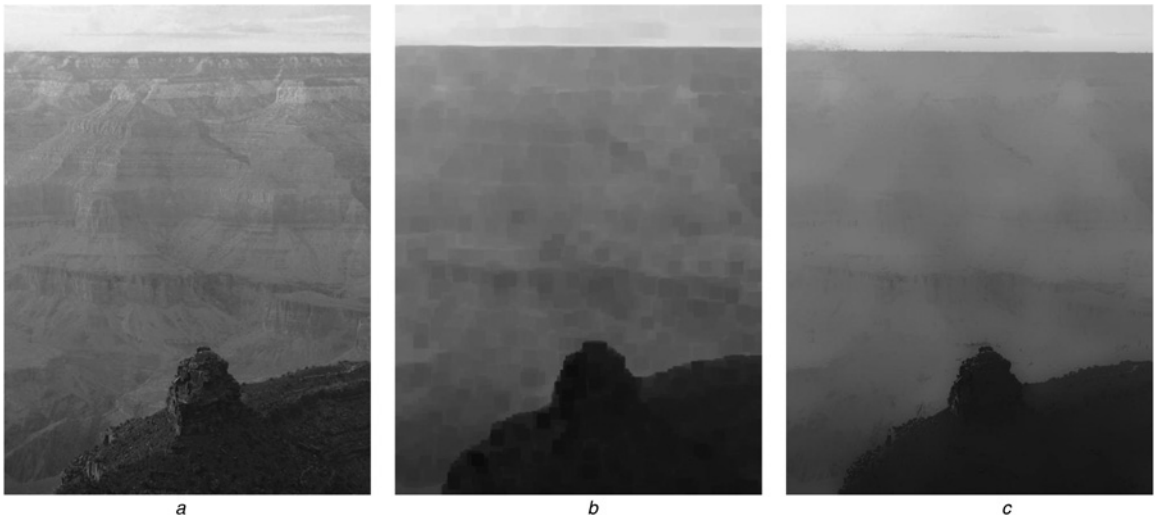

Fig. 3 *Example using the associative filter*

a Minimum image
b Dark channel image with block effect
c Refined dark channel image

doi: 10.1049/iet-cvi.2013.0011

3.3 Confidence evaluation

The dark channel confidence is defined based on two assumptions. First, the smaller the local luminance variation is, the less reliable the dark channel is. That is because the smooth area does not fulfill the dark channel prior. However, even if there is no luminance variation, it does not mean there is no haze at all. For example, the dark channel is completely unreliable in the smooth area where the luminance is 255, whereas it is totally reliable in the smooth area where the luminance is 0. To represent the grey level difference, we introduce the second assumption: the brighter the dark channel is, the less reliable it is.

We calculate the luminance by taking the maximum of the three colour channels, that is, $L(x, y) = \max_{c\in\{r,g,b\}} J_c(x, y)$ [23]. Similar to [24], we take the difference between the pixel luminance $L(x, y)$ and the background luminance $B(x, y)$ as the luminance variation, that is, $V(x, y) = |L(x, y) - B(x, y)|$. The background luminance $B(x, y)$ is obtained by substituting the luminance image and coarse background luminance, which is the local average of the luminance in a 15×15 local patch, into (4), respectively, for the reference image and the coarse image.

We simulate the first assumption based on the just-noticeable distortion (JND) profile of the human visual system (HVS). JND refers to the maximum luminance variation that the HVS cannot perceive [25, 26]. The JND profile is mainly related to the background luminance and is usually simplified as

$$\mathrm{JND}(x, y) = \begin{cases} T_0\left(1 - \sqrt{\dfrac{B(x, y)}{127}}\right) + 3, & \text{for } B(x, y) \le 127 \\ \gamma(B(x, y) - 127) + 3, & \text{for } B(x, y) > 127 \end{cases} \tag{11}$$

where $B(x, y)$ is the background luminance [25, 26], T_0 and γ denote, respectively, the visibility threshold when the background grey level is 0, and the slope of the line that models the function at higher background luminance. The values of T_0 and γ are found to be 17 and 3/128, respectively, [25].

It is easy to verify that the HVS perceives the luminance variation best in the situation where the background luminance is 127 [25, 26]. In other words, if the HVS cannot perceive the luminance variation where the background luminance is 127, it cannot perceive the luminance variation in the other situations either. Moreover, the background luminance is approximately linear to the luminance variation since the pixel luminance is linear to the background luminance [27]. Assuming that $V_{\mathrm{best}}(x, y)$ indicates the JND value where the background luminance is 127, we can obtain (12) and (13) accordingly. In order to detect the maximum amount of details, we use $V_{\mathrm{best}}(x, y)$ and 127 instead of the real $V(x, y)$ and $B(x, y)$ for further computation

$$\frac{V(x, y)}{B(x, y)} = \frac{V_{\mathrm{best}}(x, y)}{127} \tag{12}$$

$$V_{\mathrm{best}}(x, y) = 127\frac{V(x, y)}{B(x, y)} \tag{13}$$

According to the first assumption, the dark channel is reliable if the luminance variation is more than the JND value while the confidence should decrease sharply as the luminance variation becomes less than the JND value. This is in accordance with the sigmoid function, and therefore we simulate the first assumption using the sigmoid function given by (14). Similarly, we simulate the second assumption using (15)

$$C_1(x, y) = \frac{1}{1 + \exp\left(\left(\mathrm{JND}_{\min} - V_{\mathrm{best}}(x, y)\right)/k_1\right)} \tag{14}$$

$$C_2(x, y) = \frac{1}{1 + \exp\left(\left(I_{\mathrm{dark}}(x, y) - D_{\max}\right)/k_2\right)} \tag{15}$$

where $\mathrm{JND}_{\min}$ is the minimum value of the JND profile, that is, $\mathrm{JND}_{\min} = 3$, $D_{\max}$ is the maximum value of the dark channel $I_{\mathrm{dark}}(x, y)$, k_1 and k_2 are empirically set as $k_1 = 8$ and $k_2 = D_{\max}/8$.

In general, the dark channel is reliable in the situation where the local area has obvious luminance variation or the dark channel is very low. Therefore we empirically derive the model of the dark channel confidence given by (16), and we revise the transmission of (2) as (17)

$$C(x, y) = \max\left(C_1(x, y), C_2(x, y)\right) \tag{16}$$

$$t^{\mathrm{c}}(x, y) = 1 - I_{\mathrm{dark}}(x, y)C(x, y)/A^{\mathrm{c}} \tag{17}$$

We can see that $0 < C(x, y) < 1$. In the situation where the local area has detectable textures, the value of $C(x, y)$ tends to be 1, so that the revised transmission is similar to that of [9] and we can remove the haze completely. In the smooth areas, the value of $C(x, y)$ decreases as the luminance increases, so that the revised transmission becomes higher and we can prevent bringing artefacts into the smooth areas.

3.4 Airlight evaluation and haze removal

Similar to the method of [9], we pick the top 10% brightest pixels in the dark channel, and take their luminance average as the airlight in each colour channel, respectively, indicated by A^{r}, A^{g} and A^{b}. As the transmissions of different colour channels are similar for the same pixel, we substitute the average $\bar{A} = \left(A^{\mathrm{r}} + A^{\mathrm{g}} + A^{\mathrm{b}}\right)/3$ into (17) to derive the transmission $\bar{t}(x, y)$

$$\bar{t}(x, y) = 1 - I_{\mathrm{dark}}(x, y)C(x, y)/\bar{A} \tag{18}$$

By substituting $\bar{t}(x, y)$ into (3) for $t^{\mathrm{c}}(x, y)$, we can obtain the restored haze-free image $J(x, y)$

$$J^{\mathrm{c}}(x, y) = A^{\mathrm{c}} + \frac{I^{\mathrm{c}}(x, y) - A^{\mathrm{c}}}{1 - I_{\mathrm{dark}}(x, y)C(x, y)/\bar{A}} \tag{19}$$

As the airlight sometimes is not white, the values A^{r}, A^{g} and A^{b} may be seriously different. In order to prevent airlight colour shift, we substitute A^{r}, A^{g} and A^{b} into (19) for A^{c}, respectively, for the three colour channels. In a word, we use the same transmission but different airlight values for the three colour channels in (19).

4 Post enhancement

Although the objective local contrast of the restored haze-free image is indeed improved, the image looks dark in global, as Fig. 4 shows. Most pixels of the restored haze-free image are of low grey levels while a small number of pixels occupy a broad range of high grey levels. We have tested many standard enhancement methods to enhance the restored haze-free image. However, these methods usually cannot

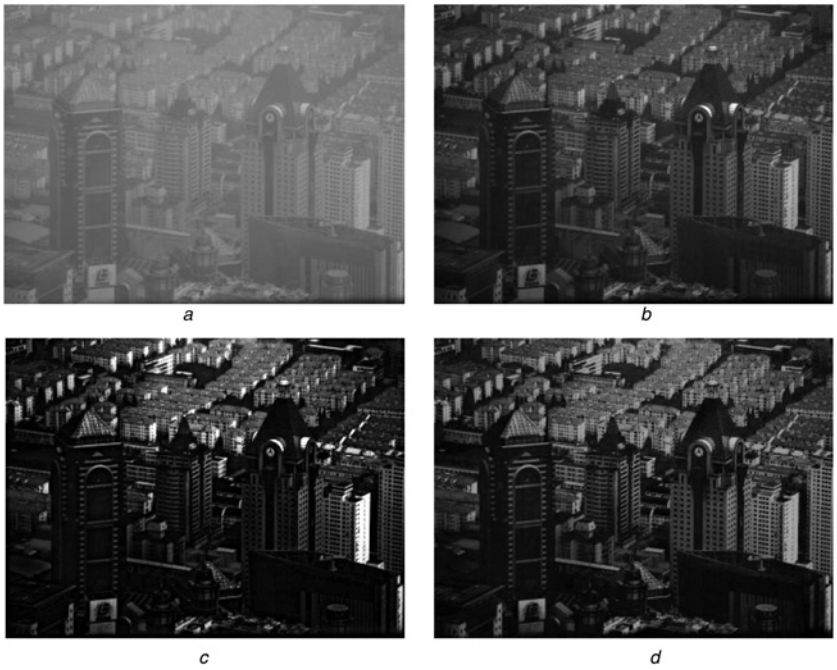

Fig. 4 *Objective local contrast of the restored haze-free image*

a Original image
b He *et al.*'s result [10]
c Result produced by Pei *et al.*'s method without post enhancement [13]
d Result produced by our method without post enhancement

make good use of the distinctive characteristics of the restored haze-free image. For example, the histogram equalisation methods usually suffer from contrast loss in the bright areas and the methods based-on Retinex usually result in over enhancement [28–31]. Therefore we propose the post enhancement method which is able to preserve the local contrast as well as extend the low grey levels.

As shown in Fig. 5, the post enhancement consists of four steps. First, we map the luminance globally to extend the low grey levels. According to [24], the local contrast depends on the ratio of each pixel's luminance to the background luminance. We estimate the ratio of each pixel to the local maximum before and after global mapping in the second step, and we restore the local contrast by restoring the ratio of each pixel to the local maximum in the third step. Finally, in order to preserve the tone, we enhance each colour channel according to the scaling of the luminance image.

We obtain the luminance image by taking the maximum of the three colour channels for each pixel

$$L(x, y) = \max_{c\in\{\mathrm{r,g,b}\}} J^{\mathrm{c}}(x, y) \tag{20}$$

We map the luminance image $L(x, y)$ globally using the method of [28], which is effective to preserve the naturalness of the image, as follows

$$L^{\mathrm{m}}(x, y) = \left(1 - \frac{1}{2}\frac{L(x, y)}{L_{\max}}\right)L(x, y) \tag{21}$$

where $L^{\mathrm{m}}(x, y)$ indicate the mapped luminance image, $L_{\max}$ is the maximum value of $L(x, y)$.

We obtain the coarse local maximum image by taking the local maximum of the luminance image. Then we calculate the refined local maximum image $L_{\mathrm{bright}}(x, y)$ using the associative filter, by substituting the luminance image and coarse local maximum image into (4), respectively, for the reference image and the coarse image. We obtain the mapped version of $L_{\mathrm{bright}}(x, y)$ as

$$L^{\mathrm{m}}_{\mathrm{bright}}(x, y) = \left(1 - \frac{1}{2}\frac{L_{\mathrm{bright}}(x, y)}{L_{\max}}\right)L_{\mathrm{bright}}(x, y) \tag{22}$$

The ratio of the pixel luminance at (x, y) to the local maximum before and after global mapping is given, respectively, by

$$R(x, y) = \frac{L(x, y)}{L_{\mathrm{bright}}(x, y)} \tag{23}$$

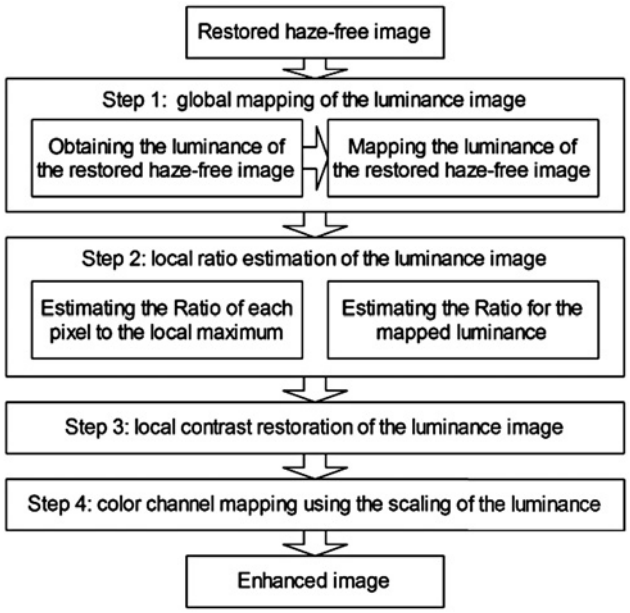

Fig. 5 *Flowchart of the post enhancement method*

doi: 10.1049/iet-cvi.2013.0011

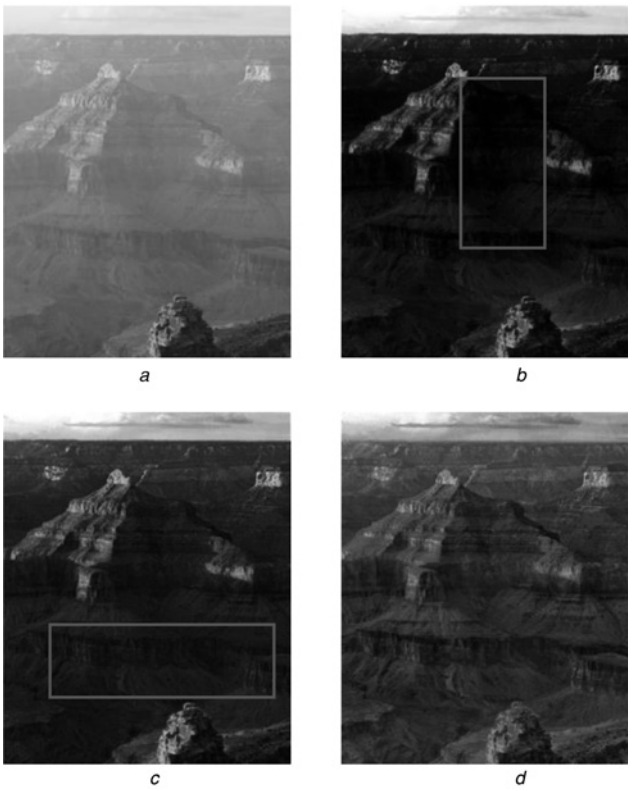

Fig. 6 *Detail comparison*
a Input image
b Fattal's result [11]
c He *et al.*'s result [10]
d Our result

$$R^{\mathrm{m}}(x, y) = \frac{L^{\mathrm{m}}(x, y)}{L^{\mathrm{m}}_{\mathrm{bright}}(x, y)} \tag{24}$$

As the local contrast of the luminance image may be reduced after global mapping, especially in the areas of high grey levels, the proposed enhancement method obtains the final enhanced luminance $L_{\mathrm{ehc}}(x, y)$ by restoring the ratio of each pixel to the local maximum

$$L_{\mathrm{ehc}}(x, y) = L^{\mathrm{m}}(x, y)\frac{R(x, y)}{R^{\mathrm{m}}(x, y)} \tag{25}$$

The scaling of the final enhanced luminance to the original restored haze-free luminance is

$$S(x, y) = \frac{L_{\mathrm{ehc}}(x, y)}{L(x, y)} \tag{26}$$

As the scaling of three colour channels is the same as that of the luminance, for each colour channel of the restored haze-free image $J(x, y)$, the enhanced version $J_{\mathrm{ehc}}(x, y)$ is obtained by the same scaling $S(x, y)$ as follows

$$J^{\mathrm{c}}_{\mathrm{ehc}}(x, y) = J^{\mathrm{c}}(x, y)S(x, y) \tag{27}$$

5 Experimental results and discussion

We compared our method with some state-of-the-art methods, including Tan's method [11], Fattal's method [10], Tarel's method [19] and two other methods using the dark channel prior [9, 12]. The evaluations are performed in terms of three criteria, details, colour naturalness and artefacts. In addition, we test the post enhancement method on the restored haze-free images compared with CHE [29] and GUM [30].

First, we validate our method based on how well our method enhances the details. From Figs. 6*b* and *c*, we can see that Fattal's method [10] and He *et al.*'s method [9] remove the haze completely, but the details of their restored haze-free images are not easy to observe in the dark areas

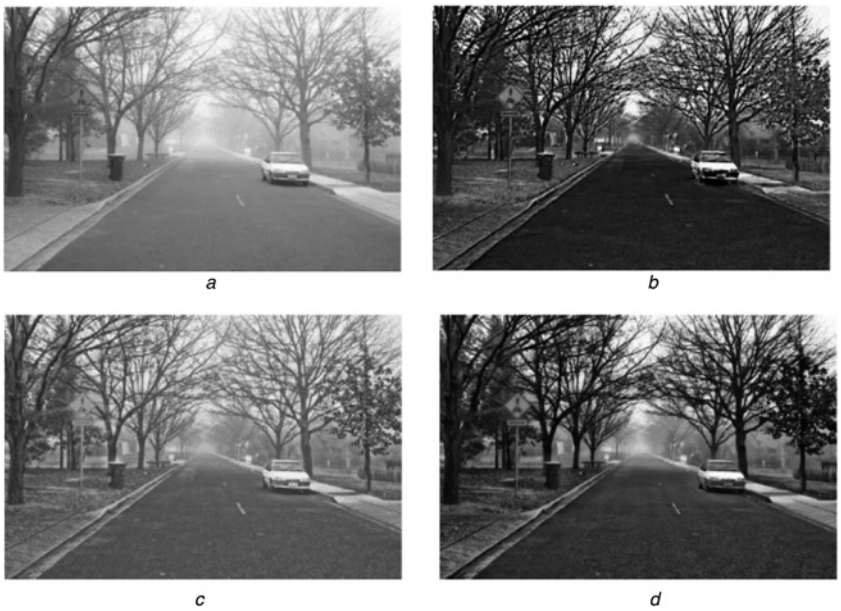

Fig. 7 *Details and saturation comparison*
a Input image
b Tan's result [12]
c Tarel *et al.*'s result [20]
d Our result

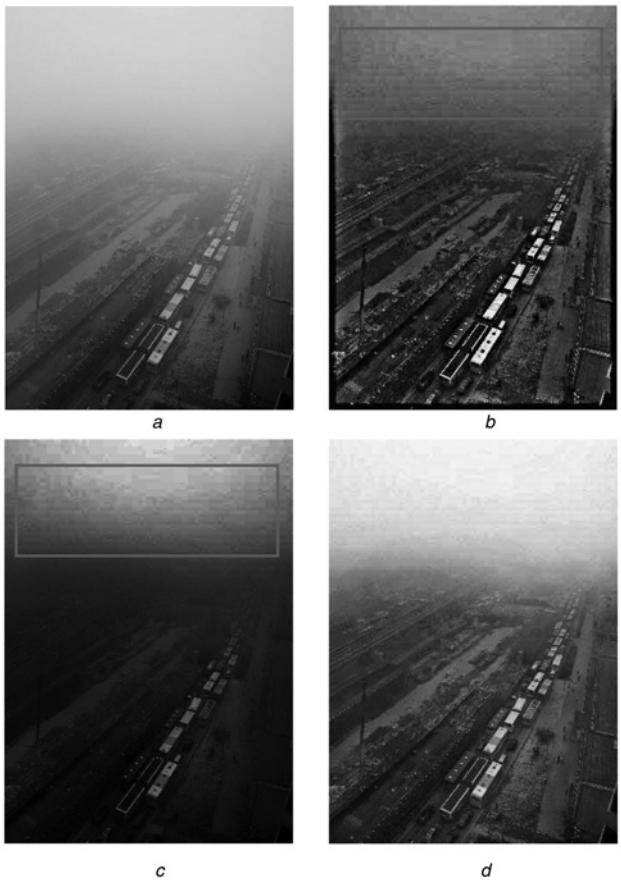

Fig. 8 *Artefacts comparison*

a Input image
b Pei *et al.*'s result [13]
c He *et al.*'s result [10]
d Our result

marked by rectangles. On the contrary, the branches of Fig. 7*c* are blurry in that Tarel *et al.*'s method [19] cannot remove the haze thoroughly. As Figs. 6*b* and *c* show, our method not only removes the haze thoroughly, but also highlights the details naturally.

Secondly, we evaluate the proposed method based on how well our method preserves the colour naturalness. He *et al.*'s method [9] and Pei *et al.*'s method [12] remove the haze by simply reducing the dark channel to zero, so that their results tend to be over saturated, as Figs. 8*b*, *c*, 9*b* and *c* show. Tan's method [11] sometimes suffers from serious hue-shift, as Fig. 7*b* shows. Comparatively, our method takes into consideration the dark channel confidence, so that the colour of our results looks natural.

Finally, we test our method based on how well our method prevents the artifacts. Both the two input images in Figs. 8 and 9 are heavily compressed by JEPG and seriously degraded because of atmospheric scattering. From the two groups of images, we can see that both the compared methods result in serious blocking effects in the areas marked by rectangles. As our method employs the dark channel confidence, there is no serious blocking effect in Figs. 8*d* and 9*d*, and the degree of the processing varies naturally between the smooth areas and the textured areas.

Finally, we compare the post enhancement method with CHE [29] and GUM [30]. For fair comparison, all the methods are tested on the restored haze-free images obtained by He *et al.*'s method [9]. CHE may cause contrast loss in the bright areas, as the marked roof area shows in Fig. 10*c*. Also, CHE cannot enhance different areas effectively. For instance, the area marked by rectangles in Fig. 11*c* remains dark. On the contrary, Fig. 10*d* is too bright to be natural. And GUM may result in over-enhancement, as the sky area in Fig. 11*d* shows. Comparatively, the luminance of our results is natural and the details are obvious.

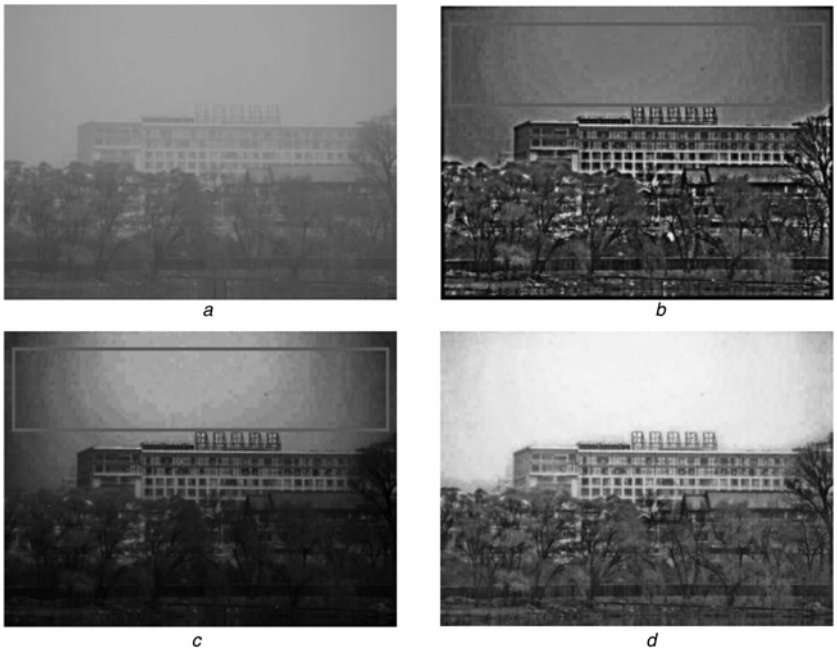

Fig. 9 *Artefacts comparison*

a Input image
b Pei *et al.*'s result [13]
c He *et al.*'s result [10]
d Our result

doi: 10.1049/iet-cvi.2013.0011

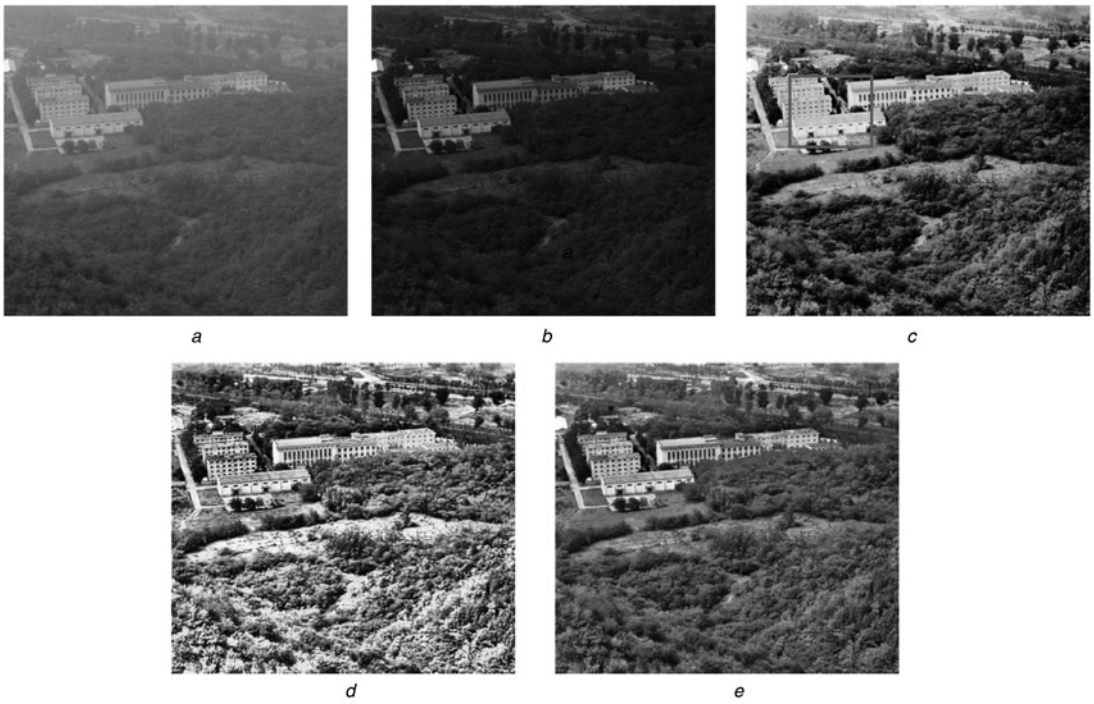

Fig. 10 *Enhancement comparison*

a Input image
b Restored haze-free image processed by He *et al.* [10]
c Enhanced version of *b* obtained using CHE
d Enhanced version of *b* obtained using GUM
e Our enhanced version of *b*

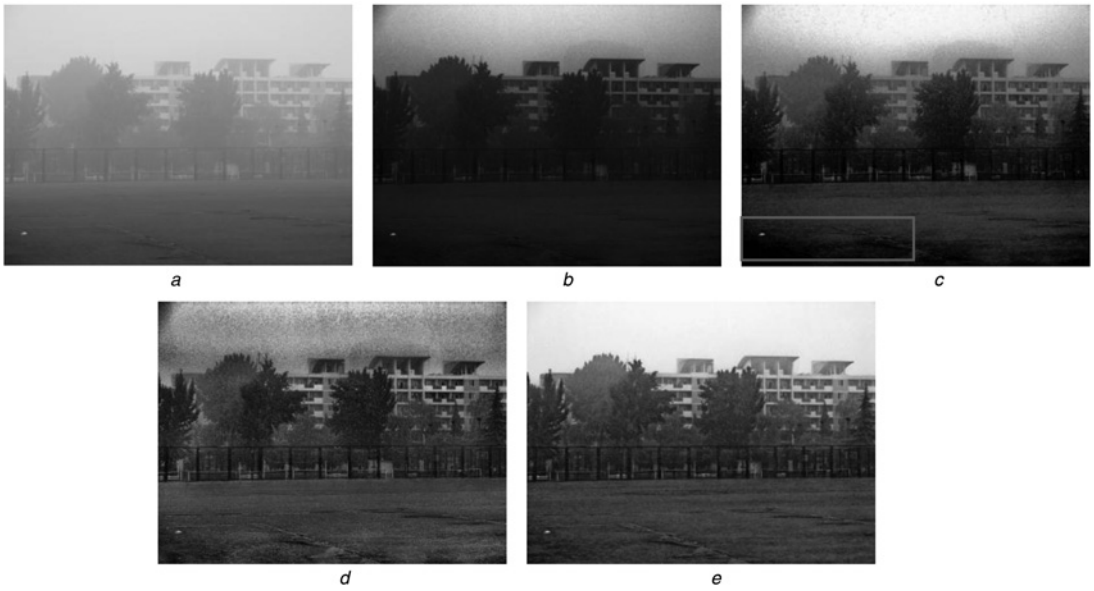

Fig. 11 *Enhancement comparison*

a Input image
b Restored haze-free image processed by He *et al.* [10]
c Enhanced version of *b* obtained using CHE
d Enhanced version of *b* obtained using GUM
e Our enhanced version of *b*

6 Conclusions

In this paper, we have proposed the method of single image haze removal using content-adaptive dark channel and post enhancement. Our method improves the existing methods from three perspectives. First, our method overcomes the problem of over-saturation by considering that the dark channel should be no brighter than the minimum colour channel. Secondly, the dark channel confidence is utilised to prevent bringing artefacts into the smooth areas. Finally,

the proposed enhancement method enhances the restored haze-free image with the local contrast preserved. Experimental results on varied images demonstrate that our method cannot only remove the haze effectively but also enhance the details significantly.

Since haze removal is highly desired in computer vision applications, it is necessary to make a further effort to put the proposed method into real-time applications, such as the video-surveillance systems and the in-vehicle vision systems. In these situations, it is necessary to take into consideration the hardware environment of the real-time systems. We leave this problem for our future research.

7 Acknowledgments

This work is supported by the National Science Fund for Distinguished Young Scholars (61125206) and the 973 Program (Project No. 2010CB327900). The authors would like to thank Jacob D'Avy and Kyle Goodrick for their helpul feedback. Special thanks go to the anonymous reviewers of this paper for their constructive comments.

8 References

1 Guan, Y.-P.: 'Spatio-temporal motion-based foreground segmentation and shadow suppression', *IET Comput. Vis.*, 2010, **4**, (1), pp. 50–60
2 Xu, M., Ellis, T., Godsill, S.J., Jones, G.A.: 'Visual tracking of partially observable targets with suboptimal filtering', *IET Comput. Vis.*, 2011, **5**, (1), pp. 1–13
3 Yilmaz, A., Javed, O., Shah, M.: 'Object tracking: a survey', *ACM Comput. Surv.*, 2006, **38**, (4), pp. 1–3
4 Narasimhan, S.G., Nayar, S.K.: 'Vision and the atmosphere', *Int. J. Comput. Vis.*, 2002, **48**, pp. 233–254
5 Shwartz, S., Namer, E., Schechner, Y.Y.: 'Blind haze separation'. Proc. IEEE Conf. Computer Vision and Pattern Recognition, 2006, vol. 2, pp. 1984–1991
6 Schaul, L., Fredembach, C., Susstrunk, S.: 'Colour image dehazing using the near-infrared'. Proc. IEEE Int. Conf. Image Processing, Cairo, Egypt, 2009, pp. 1629–1632
7 Narasimhan, S.G., Nayar, S.K.: 'Contrast restoration of weather degraded images', *IEEE Trans. Pattern Anal. Mach. Intell.*, 2003, **25**, (6), pp. 713–724
8 Wei, Y., Dong, Z., Wu, C.: 'Depth measurement using single camera with fixed camera parameters', *IET Comput. Vis.*, 2012, **6**, (1), pp. 29–39
9 He, K., Sun, J., Tang, X.: 'Single image haze removal using dark channel prior', *IEEE Trans. Pattern Anal. Mach. Intell.*, 2011, **33**, (12), pp. 2341–2353
10 Fattal, R.: 'Single image dehazing'. Proc. ACM SIGGRAPH, NY, USA, 2008, pp. 1–9
11 Tan, R.: 'Visibility in bad weather from a single image'. Proc. IEEE Conf. Computer Vision and Pattern Recognition, June 2008, pp. 1–8
12 Pei, S., Lee, T.: 'Effective image haze removal using dark channel prior and post-processing'. Proc. IEEE Int. Symp. Circuits and System, May 2012, pp. 2777–2780
13 Xie, B., Guo, F., Cai, Z.: 'Improved single image dehazing using dark channel prior and multi-scale Retinex'. Proc. Int. Conf. Intelligent Systems and Design Engineering Application, 2010, pp. 848–851
14 Dongjun, K., Changwon, J., Bonghyup, K., Hanseok, K.: 'Enhancement of image degraded by fog using cost function based on human visual model'. Proc. IEEE Int. Conf. on Multisensor Fusion and Integration for Intelligent Systems, 2008, pp. 64–67
15 Jobson, D.J., Rahman, Z., Woodell, G.A.: 'Feature visibility limits in the non-linear enhancement of turbid images'. Proc. SPIE, Visual Information Processing XII, 2003, vol. 5108, pp. 24–30
16 Woodell, G.A., Jobson, D.J., Rahman, Z., Hines, G.D.: 'Enhancement of imagery in poor visibility conditions'. Proc. SPIE, Sensors, and Command, Control, Communications, and Intelligence Technologies for Homeland Security and Homeland Defense IV, 2005, vol. 5778, pp. 673–683
17 Vizireanu, D.N., Halunga, S., Fratu, O.: 'A grayscale image interpolation method using new morphological skeleton'. Proc. IEEE Int. Conf. Telecommunication on Modern Satellite, Cable and Broadcasting Services (TELSIKS 2003), vol. 2, pp. 519–521
18 Chu, C., Lee, M.: 'A content-adaptive method for single image dehazing', (*LNCS*, **6298**), PCM, 2011, pp. 350–361
19 Tarel, J., Hautiere, N.: 'Fast visibility restoration from a single colour or gray level image'. Proc. Int. Conf. Computer Vision, 2009, pp. 2201–2208
20 Narasimhan, S.G., Nayar, S.K.: 'Contrast restoration of weather degraded images', *IEEE Trans. Pattern Anal. Mach. Intell.*, 2003, **25**, (6), pp. 713–724
21 Xiao, C., Gan, J.: 'Fast image dehazing using guided joint bilateral filter', *Vis. Comput.*, 2012, **28**, pp. 713–721
22 Kopf, J., Cohen, M.F., Lischinski, D., Uyttendaele, M.: 'Joint bilateral upsampling', *ACM Trans. Graph.*, 2007, **26**, (3), articles no. 96
23 Smith, A.R.: 'Colour gamut transformation pairs', *Comput. Graph.*, 1978, **12**, (3), pp. 12–19
24 Peli, E.: 'Contrast in complex images', *J. Opt. Soc. Am. A*, 1990, **7**, pp. 2032–2039
25 Chou, C.-H., Li, Y.-C.: 'A perceptually tuned subband image coder based on the measure of just-noticeable-distortion profile', *IEEE Trans. Circuits Syst. Video Technol.*, 1995, **5**, (6), pp. 467–476
26 Sezan, M.I., Yip, K.-L., Daly, S.J.: 'Uniform perceptual quantization: applications to digital radiography', *IEEE Trans. Syst. Man Cybern.*, 1987, **17**, (4), pp. 622–634
27 Land, E.H., McCann, J.J.: 'Lightness and Retinex theory', *J. Opt. Soc. Am.*, 1971, **61**, (1), pp. 1–11
28 Li, B., Wang, S., Geng, Y.: 'Image enhancement based on Retinex and lightness decomposition'. Proc. IEEE Int. Conf. Image Process., 2011, pp. 3417–3420
29 Arici, T., Dikbas, S., Altunbasak, Y.: 'A histogram modification framework and its application for image contrast enhancement', *IEEE Trans. Image Process.*, 2009, **18**, (9), pp. 1921–1935
30 Deng, G.: 'A generalized unsharp masking algorithm', *IEEE Trans. Image Process.*, 2011, **20**, (5), pp. 1249–1261
31 Wang, S., Zheng, J., Hu, H., Li, B.: 'Naturalness preserved enhancement algorithm for non-uniform illumination images', *IEEE Trans. Image Process.*, 2013, doi: 10.1109/TIP.2013.2261309